

Bright, NIR-Emitting Au₂₃ from Au₂₅: Characterization and Applications Including Biolabeling

Madathumpady Abubaker Habeeb Muhammed,^[a] Pramod Kumar Verma,^[b]
Samir Kumar Pal,^{*[b]} R. C. Arun Kumar,^[c] Soumya Paul,^[c]
Ramakrishnapillai Vyomakesannair Omkumar,^{*[c]} and Thalappil Pradeep^{*[a]}

Abstract: A novel interfacial route has been developed for the synthesis of a bright-red-emitting new subnanocluster, Au₂₃, by the core etching of a widely explored and more stable cluster, Au₂₅SG₁₈ (in which SG is glutathione thiolate). A slight modification of this procedure results in the formation of two other known subnanoclusters, Au₂₂ and Au₃₃. Whereas Au₂₂ and Au₂₃ are water soluble and brightly fluorescent with quantum yields of 2.5 and 1.3%, respectively, Au₃₃ is organic

soluble and less fluorescent, with a quantum yield of 0.1%. Au₂₃ exhibits quenching of fluorescence selectively in the presence of Cu²⁺ ions and it can therefore be used as a metal-ion sensor. Aqueous- to organic-phase transfer of Au₂₃ has been carried out with fluorescence enhancement. Sol-

vent dependency on the fluorescence of Au₂₃ before and after phase transfer has been studied extensively and the quantum yield of the cluster varies with the solvent used. The temperature response of Au₂₃ emission has been demonstrated. The inherent fluorescence of Au₂₃ was used for imaging human hepatoma cells by employing the avidin–biotin interaction.

Keywords: core etching • fluorescence • gold • nanostructures • phase transfer

Introduction

Synthesis of novel nanomaterials with distinct physical and chemical properties continues to draw wide attention from

researchers. Subnanoclusters, or molecular clusters of noble metals, especially of silver^[1–4] and gold,^[5–16] are new materials with numerous possibilities. They are composed of very few atoms, with a core size in the subnanometer regime, and are very different from the metallic nanoparticles of the same element. Owing to the subnanometer core size, they cannot possess continuous density of states but have discrete electronic energy levels. They show “molecule-like” optical transitions in absorption and emission and are termed as molecular clusters. Subnanoclusters act as a bridge between atomic and nanoparticle behaviors and possess properties entirely different from these two size regimes. They show characteristic absorption features and can be distinguished from each other from their absorption profiles. Subnanoclusters exhibit strong photoluminescence and their fluorescence can be tuned from the near-infrared (NIR) region to ultraviolet by decreasing the core size. It is known that metallic nanoparticles of size 2–3 nm exhibit very weak fluorescence with quantum yields in the range of 10^{−4}–10^{−5}, which is in fact very high compared to that of bulk gold (10^{−10}).^[10] However, subnanoclusters exhibit fluorescence with a quantum yield in the range of 10^{−1}–10^{−3}.^[5] Au₂₅SG₁₈, a well-studied and the most stable cluster among the glutathione-protected gold clusters, shows a quantum yield of 1 × 10^{−3} (0.1%).^[10]

[a] M. A. H. Muhammed, Prof. T. Pradeep
DST Unit on Nanoscience (DST UNS), Department of Chemistry
Sophisticated Analytical Instrument Facility
and
Indian Institute of Technology Madras, Chennai 600 036 (India)
Fax: (+91)4422570509
E-mail: pradeep@iitm.ac.in

[b] P. K. Verma, Dr. S. K. Pal
Unit for Nanoscience and Technology, Department of Chemical
Biological and Macromolecular Sciences
Satyendra Nath Bose National Centre for Basic Sciences
Block JD, Sector III, Salt Lake, Kolkata 700 098 (India)
Fax: (+91)333353477
E-mail: skpal@bose.res.in

[c] R. C. A. Kumar, S. Paul, Dr. R. V. Omkumar
Department of Neurobiology
Rajiv Gandhi Center for Biotechnology
Thiruvananthapuram, 695014 (India)
Fax: (+91)471-2346333
E-mail: omkumar@rgeb.res.in

Supporting information for this article is available on the WWW
under <http://dx.doi.org/10.1002/chem.200901425>.

Whereas, the smaller analogues such as Au₅, Au₈, and Au₁₃, synthesized inside dendrimer cavities, are highly fluorescent with a quantum yield ranging from 0.1–0.7 (10–70%).^[5] Since subnanoclusters are highly fluorescent and biocompatible due to the lower metallic content, they hold great promise as ultrabright, biocompatible biolabels and light-emitting sources in nanoscale, and hence can be used in imaging, detection, and so on, in conjunction with therapeutics. Unlike organic dyes, they are photostable,^[17] a quality that widens their potential applications. These clusters can be readily conjugated with several biological molecules, which further enhances their application potential.^[17] They also exhibit electroluminescence at room temperature and hence provide facile routes to produce strong single-photon emitters.^[18–19]

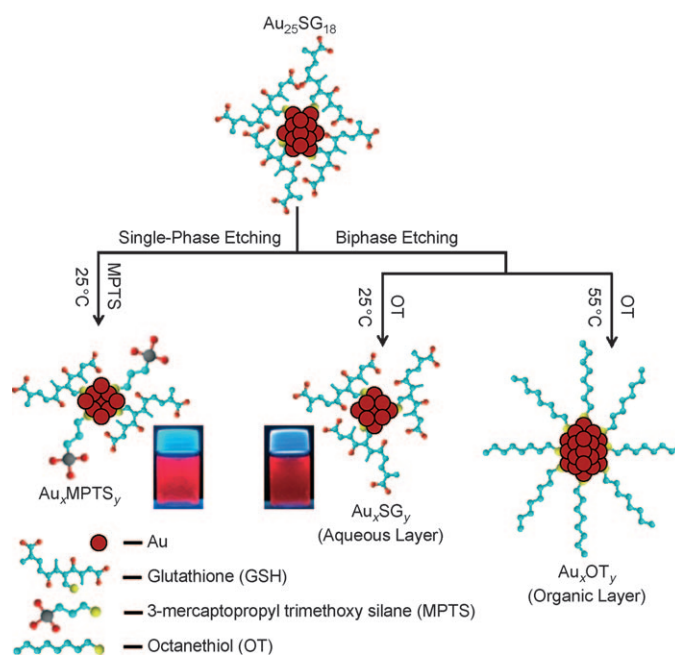
There are several methods for the synthesis of gold subnanoclusters. A group of water-soluble glutathione-protected clusters with defined chemical compositions has been synthesized by reducing Au³⁺ ions in the presence of glutathione.^[10] This produces a mixture of subnanoclusters that are the kinetically trapped intermediates of the growing Au cores. These clusters can be separated from each other by polyacrylamide gel electrophoresis (PAGE). Out of the various glutathione-protected clusters, such as Au₁₀SG₁₀, Au₁₅SG₁₃, Au₁₈SG₁₄, Au₂₂SG₁₆, Au₂₂SG₁₇, Au₂₅SG₁₈, Au₂₉SG₂₀, Au₃₃SG₂₂, and Au₃₉SG₂₄, Au₂₅SG₁₈ is the most thermodynamically stable one. The bigger clusters, $n > 25$, can be converted into Au₂₅SG₁₈ by adding excess glutathione.^[12] Templates such as dendrimers also assist in the synthesis of gold clusters. This method produces clusters of cores ranging from Au₅ to Au₃₃ by changing the Au³⁺/dendrimer ratio.^[5–7] Subnanoclusters can also be prepared from metallic nanoparticles by core etching or size reduction in the presence of excess thiols.^[20] A novel route has been developed recently for surfactant-free synthesis of fluorescent gold clusters in *N,N*-dimethylformamide.^[21] A protein-directed synthesis of highly fluorescent gold nanoclusters has also been demonstrated recently.^[22]

There is a possibility of synthesizing highly fluorescent smaller nanoclusters by the core etching of their larger analogues. With this intention, we pursued a synthetic strategy using Au₂₅SG₁₈ as the precursor. We followed two different routes for the synthesis of clusters. The first route was a biphasic or interfacial etching process that involved an organic and an aqueous phase, and the latter was a single, aqueous-phase etching process. This is the first report of the synthesis of subnanoclusters using Au₂₅SG₁₈ as the precursor. (There has been a report on the synthesis of Au₂₅ from Au₁₁.^[23]) This is also the first report of synthesis of gold subnanoclusters by interfacial etching. Interfacial synthesis is gaining attention recently as one of the promising methods for the synthesis of nanomaterials and their assemblies.^[24] Various metal nanocrystals and semiconducting materials have been synthesized using the interfacial route.^[25,26] We have recently reported the synthesis of a 7 kDa silver clusters by the interfacial route.^[27] Interfacial properties such as surface tension

and interfacial potential offer new synthetic variables to make nanomaterials.

Results and Discussion

Three distinct subnanoclusters of gold were synthesized by the core etching of Au₂₅ by treating them with an excess of thiols. Scheme 1 is a graphic representation of the formation of different clusters from Au₂₅. Two different core-etching methods, interfacial and single phase, have been followed as outlined below.



Scheme 1. Formation of the three subnanoclusters from Au₂₅SG₁₈ by core etching through two routes. Photographs of the cluster in aqueous solutions under UV light are also given.

For interfacial etching, an interface was created by making an immiscible biphasic mixture of toluene containing octanethiol (OT) and an aqueous solution of Au₂₅SG₁₈. The biphasic mixture was stirred at 25 and at 55°C, separately. A highly fluorescent, water-soluble cluster was obtained by etching at 25°C. In contrast, at 55°C, an organic-soluble cluster was seen. The formation of different clusters was characterized by monitoring the changes in optical absorption features of both the aqueous and the toluene layers. Parent Au₂₅SG₁₈ has a well-structured optical absorption profile, as shown in Figure 1, with an absorption maximum at 672 nm.^[10] The peak at 672 nm (1.55 eV) arises due to a LUMO ← HOMO transition that can be called an intraband (sp ← sp) transition. The features in the lower wavelength region arise due to an interband transition (sp ← d).^[28] During etching at 25°C, the characteristic optical absorption features of Au₂₅ started disappearing and new features started appearing in the aqueous layer. After 5 h of stirring, the

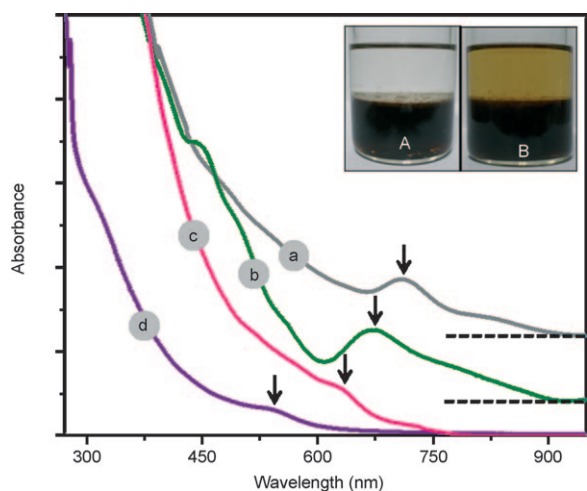


Figure 1. Comparison of the optical absorption features of b) $\text{Au}_{25}\text{SG}_{18}$ with a) Au_xOT_y , c) Au_xSG_y , and d) Au_xMPTS_y . The arrows show the absorption peaks of the clusters due to intraband transitions. The spectra are shifted vertically for clarity. Dotted lines indicate the threshold of absorption. The inset shows the photographs (under white light) of the water–toluene biphasic mixture A) before and B) after reaction at 55°C (interfacial etching) for 1 h.

optical absorption spectrum of the aqueous phase showed a feature at 630 nm and this remained the same even after a longer reaction time. The aqueous layer was centrifuged. The supernatant contained the cluster, and the residue was the insoluble $\text{Au}^{\text{I}}\text{SG}$ polymer that was formed due to the etched gold atoms. (The cluster formed by this method will be called Au_xSG_y in the following discussion.) The toluene layer remained almost colorless and did not show any significant absorption feature. Au_xSG_y was subjected to PAGE (data not shown), which shows only one fluorescent band; this suggests the formation of only one type of cluster. On the other hand, at 55°C the toluene layer, which was colorless initially, turned light brown (see inset of Figure 1). After 1 h of stirring, the optical absorption spectrum of the toluene layer was measured. It showed a well-defined absorption feature, with an absorption maximum at 709 nm. This corresponds to the formation of a well-defined cluster with a core in the subnanometer regime. The toluene layer was centrifuged to remove any insoluble deposits. (The cluster formed in the organic phase by this method will be called Au_xOT_y in the following discussion.) We will show later in the text that only one kind of cluster is present in this phase and therefore this classification. There was, however, a deposition of insoluble gold(I) thiolate in the aqueous layer. Upon its removal, this phase was colorless.

For single-phase etching, 3-mercaptopropyl trimethoxy silane (MPTS) was added to the aqueous solution of Au_{25} and stirred for 7 h at 25°C . During etching, the color of the aqueous layer became increasingly reddish compared with that of Au_{25} . After 7 h of etching, the solution showed an absorption peak at 540 nm and the characteristic features of Au_{25} disappeared completely. This solution was centrifuged

to separate the cluster from the insoluble gold thiolate. (This cluster formed will be called Au_xMPTS_y in the following discussion, again due to the fact that only one kind of cluster is present.)

The mechanism of formation of the clusters is not well understood. We present below our tentative suggestion for the formation of clusters. Etching of gold nanoparticles by excess thiols is known.^[12–15,20] During interfacial etching at 25°C , octanethiol etches Au_{25} at the water–toluene interface and the etched gold atoms along with some glutathione ligands form $\text{Au}^{\text{I}}\text{SG}$ thiolate, which precipitates. The removal of some of the gold atoms from the Au_{25} core changes the core and a new cluster is formed. But at 55°C , the gold atoms, removed from the surface of Au_{25} by excess octanethiol, come to the toluene layer as gold(I) octanethiolate because of the high temperature. Solubility of thiolates in toluene increases with temperature.^[29] Gold(I) thiolate may undergo aurophilic interactions to form the cluster, as there is a tendency for gold(I) compounds to form oligomers, chains, or layers by means of gold(I)–gold(I) interactions due to the hybridization of the empty 6s/6p and filled 5d orbitals.^[30–32] In the case of single-phase etching, both the thiol and Au_{25} are in the same phase. Therefore, etching is very easy and the amount of thiol required for etching was low (two times the glutathione ligand present on Au_{25}) when compared with interfacial etching (eight times). Absorption features of all the three clusters synthesized from Au_{25} are completely different from each other and also from the parent Au_{25} , which makes it easy to distinguish them.

A thorough analysis of the optical absorption features of the clusters showed that the absorptions due to HOMO–LUMO transitions, which are marked by arrows, shed some light on the core size of the product clusters. Tsukuda et al. showed that the absorption peaks due to HOMO–LUMO transitions show a blueshift with a decrease in core size.^[10] As the size decreases, the spacing between discrete states in each band increases, and that leads to blueshift in the absorption of smaller clusters when compared with the larger analogues. From this, it can be suggested that the core size of the clusters decreases in the order $\text{Au}_x\text{OT}_y > \text{Au}_{25}\text{SG}_{18} > \text{Au}_x\text{SG}_y > \text{Au}_x\text{MPTS}_y$. The absorption peaks were at 709, 672, 630, and 540 nm, respectively. A closer look at the absorption features suggested that the absorption profiles of Au_xOT_y and Au_xMPTS_y matched with the absorption profiles of $\text{Au}_{33}(\text{SG})_{22}$ and $\text{Au}_{22}(\text{SG})_{17}$, respectively. $\text{Au}_{33}(\text{SG})_{22}$ and $\text{Au}_{22}(\text{SG})_{17}$ were separated by PAGE from a mixture of glutathione-capped clusters.^[10] $\text{Au}_{33}(\text{SG})_{22}$ and $\text{Au}_{22}(\text{SG})_{17}$ showed absorption features at 710 and 540 nm, respectively. From this, we can tentatively assign a core of Au_{22} to Au_xMPTS_y and Au_{33} to Au_xOT_y . We also know that a change in the ligand does not influence the nature of the absorption spectrum significantly.^[14] Conversely, Au_xSG_y which has an absorption peak at 630 nm, is expected to have a core between Au_{25} and Au_{22} . A cluster with this absorption profile has not been reported so far.

To find the nature of the core of Au_xSG_y , mass spectrometric analysis was carried out using matrix-assisted laser-

desorption ionization (MALDI) mass spectrometry. However, electrospray ionization mass spectrometry (ESIMS) in the orthogonal geometry as in ours does not give features due to intact clusters as reported previously.^[10] α -Cyano-4-hydroxycinnamic acid (CHCA) was used as the matrix. The spectrum was collected in the negative mode. The mass spectrum shows a bunch of peaks with m/z values ranging from 100 to 10000 (Figure 2A). Peaks at low m/z regions are very intense with huge background signals when compared to those at higher m/z values. There is a pattern of

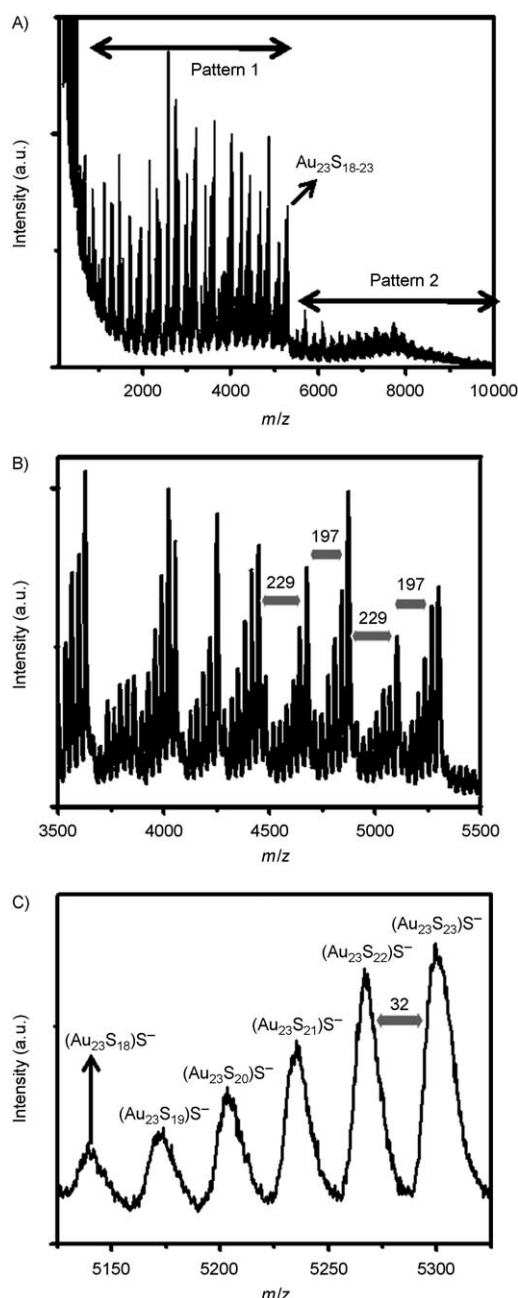


Figure 2. A) MALDI-MS of Au_xSG_y , showing a bunch of peaks due to Au_mS_n clusters. B) A group of peaks with m/z spacing of 197 or 229 between the major peaks of the adjacent group of peaks. C) Expanded view of peaks due to $Au_{23}S_{18-23}$.

peaks between m/z 1800 and 5300 and another pattern from m/z 5500 to 9000. The second set of peaks can be due to the clustering of ions detected in the lower m/z values. Clustering of clusters is observed in MALDI-MS studies of clusters.^[33] The mass spectrum is composed of several groups of peaks with spacing of m/z 197 or 229 between the major peaks, as shown in Figure 2B. This corresponds to the loss of Au or AuS. The m/z spacing between isolated peaks in each cluster of peaks is 32 on account of sulfur. These results are consistent with the earlier reports of laser-desorption mass spectrometry of gold clusters protected with thiolates.^[34] Each bunch of peaks can be assigned as $[Au_mS_n]^-$. Since laser irradiation cleaves the S-C bond of the ligands, we can observe only peaks due to Au_m clusters covered with S, and not the entire ligand. The last group of peaks of pattern 1 is due to $Au_{23}S_{18-23}$ (Figure 2A). It is worth noting that after the peak due to Au_{23} , the intensity drops drastically. The major peak at m/z 5140 can be assigned $(Au_{23}S_{18})S^-$; then addition of S leads to $(Au_{23}S_{19})S^-$, $(Au_{23}S_{20})S^-$, and so on (Figure 2C). Such additions are observed in MALDI and LDI. From these, we can tentatively assign a core of Au_{23} for the Au_xSG_y cluster.

The nature of the ligand protection of the clusters can be studied using their FTIR spectra, which will give features due to the ligands. FTIR spectra of the three clusters were compared with those of parent $Au_{25}SG_{18}$ and the ligands used for etching (see Figure S1 in Supporting Information 1). FTIR spectra of the ligands bound on the cluster surface are less intense than the free ligands, owing to the fact that these ligands are linked to the cluster surface through covalent bonds. They are also distributed nonuniformly on the cluster surfaces, hence their vibrational features are masked to some extent. FTIR spectra of $Au_{25}SG_{18}$ and Au_xSG_y match exactly with each other and therefore it can be concluded that the Au_xSG_y clusters are protected completely with glutathione as in $Au_{25}SG_{18}$, which makes them water soluble. The peak at 2526 cm^{-1} due to the -SH stretching of glutathione disappeared both in $Au_{25}SG_{18}$ and in Au_xSG_y , thereby suggesting the covalent bonding of glutathione with the cluster core through the thiolate link. The FTIR spectrum of Au_xOT_y shows features due to octanethiol. The peak at 2568 cm^{-1} due to the -SH stretching mode of octanethiol disappeared in Au_xOT_y , confirming the covalent binding of octanethiol with the cluster core through the -SH group. The presence of OT on the cluster surface can also be confirmed by the large intensity of the -CH₂ stretching modes at 2846 and 2918 cm^{-1} . Since single-phase etching was carried out in water, 3-mercaptopropyl trimethoxysilane underwent hydrolysis to 3-mercaptopropyl trisilanol. FTIR spectra of Au_xMPTS_y showed features due to both 3-mercaptopropyl trisilanol and glutathione, which suggested that the cluster is protected with a mixed monolayer of 3-mercaptopropyl trimethoxysilanol and glutathione. The features due to 3-mercaptopropyl trisilanol were more significant compared with the glutathione features. The ligand protection of the clusters can now be summarized as follows. Whereas Au_xSG_y is protected with glutathione, Au_xMPTS_y is

protected with a mixed monolayer of 3-mercaptopropyl trisilanol and glutathione. Au_xOT_y is covered by octanethiol (all in thiolate form).

To check the presence of gold and other elements, energy dispersive analysis of X-rays (EDAX) was carried out (see Supporting Information 2) by drop-casting the aqueous solution of Au_xSG_y and solution of Au_xOT_y in toluene on indium–tin oxide (ITO) glass plates. Since Au_xMPTS_y was expected to have silicon, the EDAX measurements were carried out by pasting the powder of the cluster on a carbon tape. The elements present in the clusters were mapped. Whereas Au_xSG_y contained Au, C, N, O, and S, the elements present in Au_xMPTS_y were Au, C, N, O, S, and Si. The elements present in Au_xOT_y were Au, C, and S. Based on that information, the core and ligand protection of all three clusters are known. To assign chemical compositions to the clusters, elemental analyses (CHNS) were carried out. The results are given in the table in Supporting Information 2. The molecular formulae of the clusters were found to be $\text{Au}_{22}(\text{MPTS})_{10}(\text{SG})_7$, $\text{Au}_{23}(\text{SG})_{18}$, and $\text{Au}_{33}(\text{OT})_{22}$.

Figure 3 summarizes the 4f core-level photoemission spectra of Au_{22} , Au_{23} , and Au_{33} along with parent Au_{25} . The binding-energy (B.E.) position of the clusters came in the range

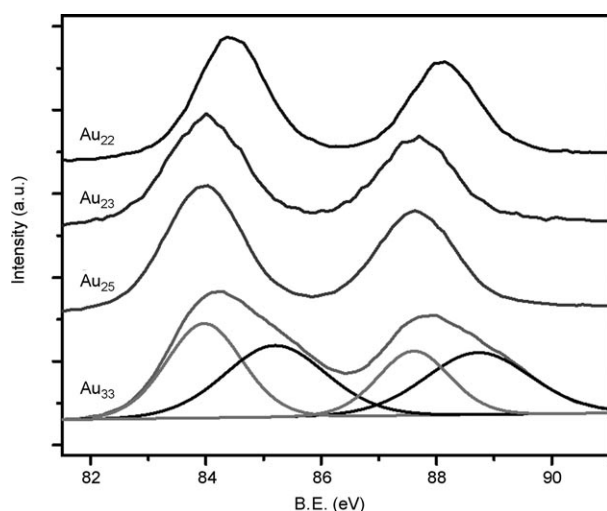


Figure 3. Comparison of the Au(4f) XPS spectra of Au_{22} , Au_{23} , and Au_{33} along with parent Au_{25} .

84.4–84.8 eV for $4f_{7/2}$ and 88.1–88.5 eV for $4f_{5/2}$. Tsukuda et al. reported that the binding energy of $4f_{7/2}$ of the glutathione-protected clusters came between 84 and 86 eV, that is, between the binding-energy values of gold film and gold thiolate.^[10] S2p, N1s, and O1s core-level photoemission spectra from the ligand moieties of the clusters are compared in Figure S3 in Supporting Information 3. Binding-energy values of S2p, N1s, and O1s of Au_{25} and Au_{23} are the same, thus indicating that both Au_{25} and Au_{23} are protected with the same ligand, that is, glutathione, which was proved by FTIR and other techniques. However, S2p, N1s, and O1s core-level photoemission spectra of Au_{22} showed a shift

from Au_{25} and Au_{23} clusters. This may be due to the mixed protection of glutathione and trisilanol. Au_{22} showed an additional peak due to Si2p on account of the silanol protection that was absent in all other clusters. Au_{33} showed only S2p and there was no intensity at N1s or O1s as expected for octanethiol protection. The S2p binding energy for Au_{25} and Au_{23} , both protected with –SG, occurs at 162.5 eV, characteristic of thiolate. The mixed monolayer-protected cluster, Au_{22} , shows, however, a higher binding energy of 163.2 eV. The OT-protected Au_{33} apparently manifests two distinct S2p states (162.8 and 163.8 eV), possibly due to the distinct chemical species at the surface. In none of these are oxidized species such as sulfonates or sulfates observed; these are characteristic of X-ray-induced damage of thiolate monolayers. This implies stability of the monolayer structure.

All three clusters exhibited fluorescence in the NIR region. The photoluminescence profiles of all the clusters along with that of parent Au_{25} are given in Figure 4. Au_{23}

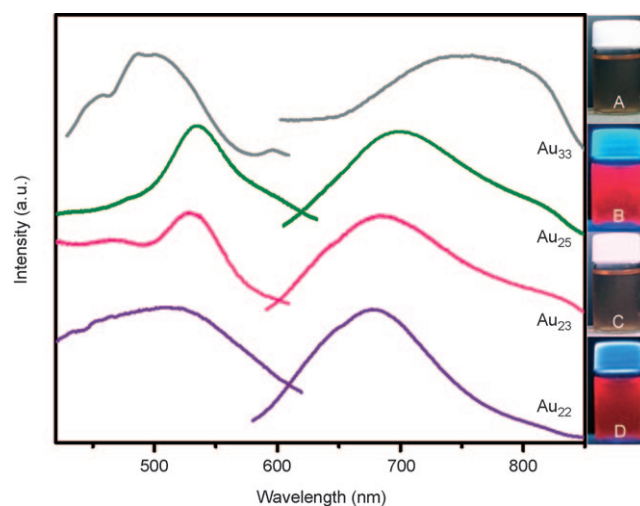


Figure 4. Comparison of the photoluminescence profiles of Au_{22} , Au_{23} , and Au_{33} along with parent Au_{25} . Photographs of the aqueous solutions of Au_{22} and Au_{23} under white light (A and C, respectively) and UV light (B and D, respectively) are also given.

and Au_{22} are brightly fluorescent and showed strong red emission when the aqueous solutions of the clusters were irradiated by a UV lamp at room temperature. Whereas, Au_{33} was weakly fluorescent and did not show any emission under the UV lamp at room temperature. The emission maxima of Au_{22} , Au_{23} , Au_{25} , and Au_{33} are 679, 685, 700, and 750 nm, respectively. The quantum yields of Au_{22} , Au_{23} , and Au_{33} were 2.5, 1.3, and 0.1%, respectively. The photoluminescence of the subnanoclusters arises due to their molecular-like electronic structure. The emission originates from radiative intraband transitions within the sp bands, across the HOMO–LUMO gap.^[6,10] The enhanced fluorescence and the quantum yield of Au_{22} and Au_{23} when compared with parent Au_{25} can be explained as follows. As the size decreases, the spacing between discrete states in each band increases,

es. That leads to a blueshift in the emission of smaller clusters when compared with the larger analogues. The emission wavelength of the clusters decreased in the order $\text{Au}_{33}\text{OT}_{22} > \text{Au}_{25}\text{SG}_{18} > \text{Au}_{23}\text{SG}_{18} > \text{Au}_{22}(\text{MPTS})_{10}(\text{SG})_7$. Lower density of states of smaller clusters minimizes internal nonradiative relaxation pathways and therefore they are more fluorescent compared to bigger ones.^[6]

Fluorescence decays of Au_{22} , Au_{23} , and Au_{25} in water and Au_{33} in toluene were measured. Data obtained using a picosecond-resolved time-correlated single-photon counting (TCSPC) technique is shown in Figure S4 in Supporting Information 4. Lifetime values of the clusters were obtained by the numerical fitting of the fluorescence at 630 nm. They are 0.04 (73.5%), 0.70 (8.2%), 6.0 (6.1%), and 95.2 ns (12.2%) for Au_{22} ; 0.04 (92.4%), 2.4 (3.6%), and 68.5 ns (4.0%) for Au_{23} ; 0.08 (78.2%), 0.4 (20.1%), 4.3 (0.9%), and 64.5 ns (0.8%) for Au_{33} ; 0.03 (96.7%), 3.6 (1.0%), and 99.3 ns (2.3%) for Au_{25} .

The clusters can be imaged using their inherent fluorescence. Fluorescence images of drop-casted Au_{23} and Au_{22} solid films were recorded using a confocal Raman spectrometer equipped with 532 nm excitation. The images in Figure 5 show fluorescence from Au_{23} - and Au_{22} -rich regions. Although there was fluorescence from the red spots, there was no fluorescence from the dark areas. The red spots are

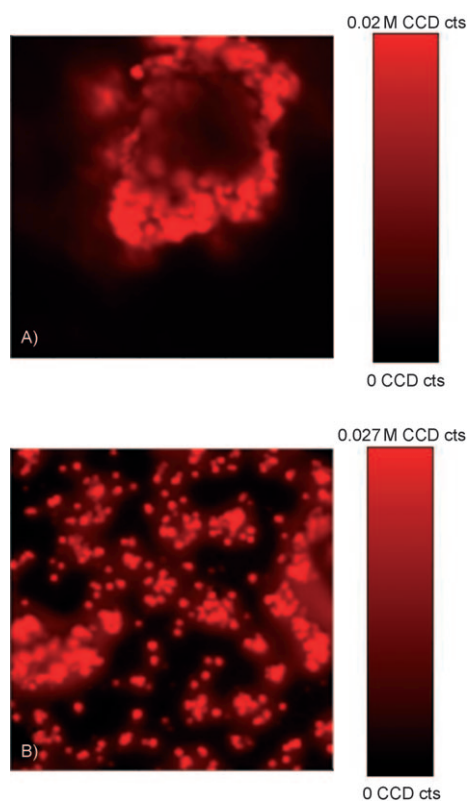


Figure 5. Inherent fluorescence image of A) Au_{22} and B) Au_{23} collected by the spectroscopic mapping at an excitation wavelength of 532 nm. Regions coded red represent the pixels where the signal (used for mapping) is a maximum, the minima being represented with black. The scan area was $40 \mu\text{m} \times 40 \mu\text{m}$.

the islands of Au_{22} or Au_{23} clusters. These images show that the clusters are also fluorescent in the solid state. Since Au_{23} is a completely new cluster and is brightly fluorescent and water soluble, we decided to investigate its properties further for various applications.

The effect of fluorescence of Au_{23} in the presence of various metal ions was studied. The ions selected were Au^{3+} , Ag^+ , Cu^{2+} , Ni^{2+} , Ca^{2+} , Mg^{2+} , Na^+ , Pb^{2+} , Hg^{2+} , and Cd^{2+} as their nitrates or chlorides. Next, 50 ppm of the aqueous solutions of Au_{23} was treated with metal ions so that the final concentration was 10 ppm, and the emissions of the clusters were measured immediately after the addition of ions. Au_{23} was found to be reactive towards Cu^{2+} . The emission of the cluster quenched significantly. Although cluster emission enhanced a bit in the presence of Ag ions, it remained unaltered in the presence of other metal ions. Figure 6 is the plot of cluster-emission intensity against the

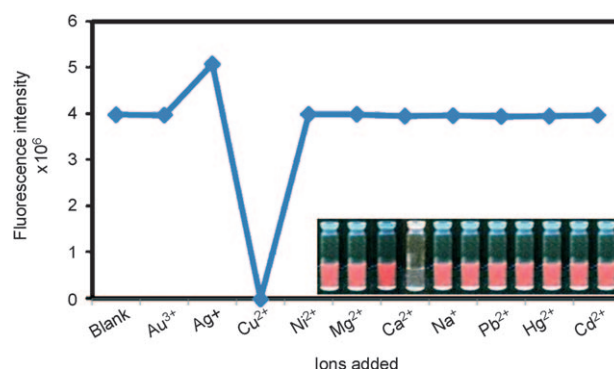


Figure 6. Plot of the fluorescence intensity of an aqueous solution of Au_{23} against the ions added externally to the solution. The concentration of Au_{23} was the same for all experiments. Clusters showed specific reactivity towards Cu ions with significant quenching of fluorescence. Photographs of the aqueous solution of Au_{23} in the presence of externally added ions under UV light irradiation are also given. The photograph was collected immediately after the addition of metal ions.

metal ions added. Inset is the photograph of the aqueous solutions of Au_{23} under UV light irradiation after the addition of various metal ions. The specific reactivity towards Cu^{2+} can be used as a detection tool to find the presence of Cu^{2+} ions. The fluorescence quenching in the presence of Cu^{2+} may be due to the complexation between glutathione and the metal ion. However, Au_{23} did not show any particular reactivity towards anions.

The Au_{23} cluster is protected with glutathione and is water soluble. The cluster can be transferred from the aqueous to the toluene phase by the phase-transfer reagent tetraoctylammonium bromide (TOABr). For this, an aqueous solution of Au_{23} was mixed with toluene containing TOABr and stirred vigorously for 2 min. Au_{23} clusters underwent immediate and complete phase transfer from the aqueous to the toluene layer. The phase transfer can be monitored visually by the color changes in the aqueous and toluene layers. The colorless toluene layer turned reddish brown and the aqueous layer, which was originally reddish brown, turned color-

less after stirring. The phase transfer occurred by the electrostatic attraction between the hydrophilic carboxylate anion of the glutathione ligand on the cluster surface in the aqueous phase and the hydrophobic tetraoctylammonium cation in the toluene phase. The phase-transferred cluster is believed to be protected with glutathione monolayer and covered by TOA⁺. This covering of TOA⁺ makes the cluster hydrophobic and results in its transfer from the aqueous to the toluene layer. The phase-transferred cluster was very stable when compared with the aqueous solution. The optical absorption profile of the cluster remained the same after phase transfer and this suggested that the cluster retained its core after phase transfer (see Figure S5A in Supporting Information 5). The emission of the cluster enhanced significantly after phase transfer. The photoluminescence profiles of the cluster before and after the phase transfer are given in Figure 7. Photographs of the biphasic mixture before and

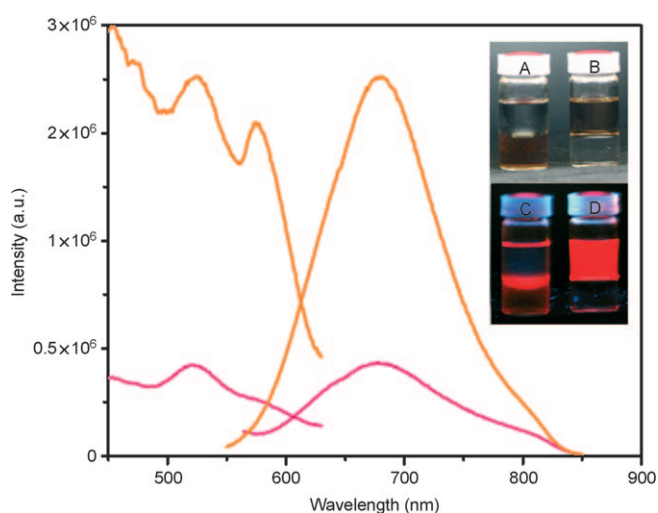


Figure 7. Photoluminescence profile of Au₂₃ cluster before (—) and after (—) phase transfer. Emission of the cluster enhances considerably after the phase transfer. Photographs of the aqueous toluene mixture containing the cluster before and after phase transfer under white light (A and B, respectively) and UV light (C and D, respectively). In C, only the interface is illuminated; the UV is attenuated as the sample was irradiated from the top.

after phase transfer under white light and UV light irradiation are also shown. Intensity of the onset in the excitation profile of the cluster around 575 nm enhanced enormously. The quantum yield of the cluster after phase transfer was increased to 5%. To understand the reason for the enhancement of fluorescence, we calculated the radiative (k_r) and nonradiative (k_{nr}) decay rate constant using the relation shown in Equation (1):^[35]

$$\Phi = k_r / (k_r + k_{nr}) = k_r \tau \quad (1)$$

in which Φ and τ are the quantum yield and average fluorescence lifetime, respectively. Both the k_r and k_{nr} rates of the cluster Au₂₃ are altered on phase transfer, thus indicating a

change in the kinetics of electron-hole recombination (Table 1). The decrease in k_{nr} rate is significant upon phase transfer to an organic medium and can be explained as fol-

Table 1. Tabulation of radiative and nonradiative decay rates of Au₂₃ in water, toluene, dioxane, and ethylene glycol. The first two datasets compare the values before and after phase transfer.

Solvents	Φ	τ [ns]	k_r [10^7 s ⁻¹]	k_{nr} [10^7 s ⁻¹]
water	0.013	0.4	3.250	246.75
toluene (phase-transferred)	0.050	2.6	1.900	36.10
dioxane	0.001	6.5	0.015	15.38
ethylene glycol	0.045	10.6	0.420	8.91

lows. The ability of thiols to act as hole traps is well known.^[36] In the organic phase, further passivation of the cluster by TOA⁺ makes the glutathione (thiols) less active and hence the decrease in nonradiative decay can be attributed to the reduced ability of thiols to act as hole traps for the cluster. Fluorescence decay of the cluster after phase transfer was measured (see Figure S5B in Supporting Information 5). Lifetimes of the cluster before and after phase transfer are given in the table in Supporting Information 5. The percentage of the faster component decreased after the phase transfer; this is a consequence of reduction in nonradiative decay. Phase transfer promises several possibilities to explore the properties, reactivity, and applications of subnanoclusters both in the aqueous and organic phases.

The temperature-dependent emission of Au₂₃ cluster was studied both in the aqueous and in the toluene phases (i.e., before and after phase transfer). Cluster emissions were collected at different temperatures of 5, 15, 25, 40, 50, and 60 °C (Figure 8). At higher temperatures, the cluster decom-

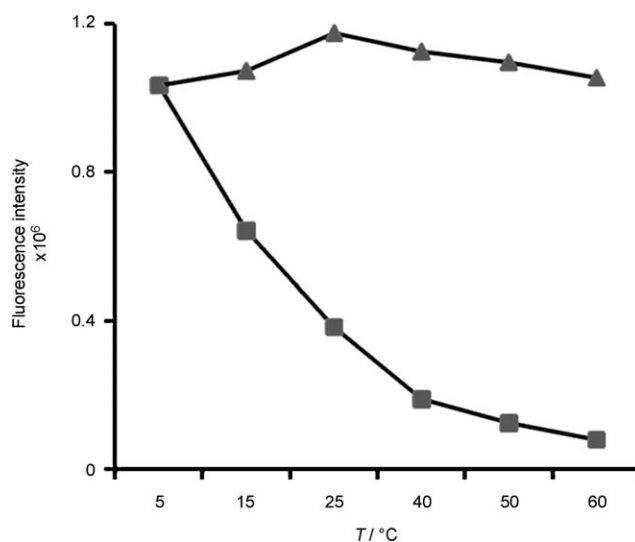


Figure 8. Plot of temperature versus fluorescence intensity of the cluster in the aqueous (■) and toluene (▲) layers. Whereas the intensity of emission of aqueous solution of Au₂₃ decreases with an increase in temperature, the emission intensity remains unaltered for phase-transferred Au₂₃.

poses and the study could not be extended beyond 60 °C. Emission of the cluster in the aqueous phase decreased significantly upon increase in temperature. However, emission of the cluster in the toluene phase remained more or less the same at different temperatures. The reason for the decrease in the intensity of the cluster in the aqueous phase can be explained in terms of hydrogen bonding. A hydrogen bond exists between the ligands of the clusters and between the ligand and water in the aqueous medium. Stability of the hydrogen bond is very sensitive to temperature. The extent of hydrogen bonding increases with a decrease in temperature. At a higher temperature, molecular motion increases and density decreases. But at lower temperatures, molecular motions are arrested to some extent and the density increases. A phase-transferred cluster, on the other hand, can be considered core-shell material with TOA⁺ coating on Au₂₃SG₁₈. As the cluster is in toluene, there is no chance of any hydrogen bonding and the fluorescence of the cluster remains unaltered by temperature variation.

The influence of the solvents on the fluorescence of Au₂₃ was studied. The solvents in which fluorescence is measured play a crucial role in determining the fluorescence intensities as well as wavelength of emission. The position of fluorescence maximum in one solvent relative to the other depends on the relative separations between ground and excited states in either solvent and therefore relative strengths of ground and excited-state solvent stabilization.^[37] The solvents selected were dioxane, acetonitrile, water, methanol, and ethylene glycol based on their hydrogen-bonding capacity. Water, methanol, and ethylene glycol can form hydrogen bonds with the cluster through glutathione, with a maximum in ethylene glycol and minimum in water. Dioxane and acetonitrile, however, have no hydrogen-bonding capacity. For the solvent dependent emission study, 0.5 mL of the aqueous solution of the cluster was mixed with 1.5 mL of the solvents. The emission of the cluster enhanced in the following order: dioxane < acetonitrile < water < methanol < ethylene glycol (Figure 9A). The quantum yields were 0.1, 0.2, 1.3, 3, and 4.5%, respectively, in these solvents. Since dioxane has no hydrogen-bonding capacity, the cluster emission was quenched when compared with the aqueous solution, and emission of the cluster enhanced in ethylene glycol because of the two OH groups per molecule participating in hydrogen bonding. The optical absorption profile of the cluster remained the same in all the solvents, which suggested the retention of cluster core in all the solvents (see Figure S6A in Supporting Information 6). There was a blueshift in the emission of the cluster in methanol and ethylene glycol. To understand how solvents alter the quantum yield of the cluster, picosecond-time-resolved photoluminescence measurements were carried out. The time-resolved studies (see Figure S6B in Supporting Information 6) showed that the percentage of the faster component decreases from dioxane to ethylene glycol (see the table in Supporting Information 6), which again signifies a reduction in nonradiative decay due to additional stability gained by cluster on account of hydrogen bonding. These hydrogen

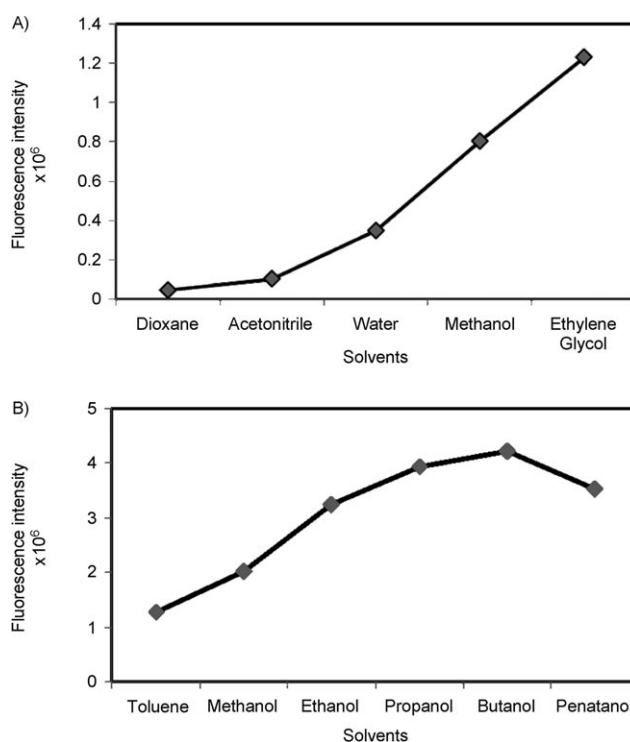
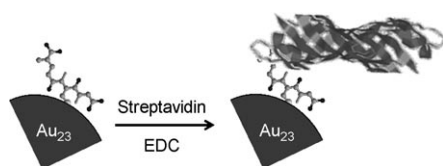


Figure 9. A) Solvent-dependent fluorescence of 50 μM Au₂₃ in ethylene glycol, methanol, water, acetonitrile, and dioxane before phase transfer. B) Solvent-dependent fluorescence of Au₂₃ in methanol, ethanol, propanol, butanol, and pentanol after phase transfer.

bonds provide additional passivation of the Au₂₃ cluster, thereby making glutathione (thiols) less efficient in acting as hole traps. From the steady-state quantum yield and fluorescence lifetime values, k_r and k_{nr} decay rate constants were calculated. Table 1 is the tabulation of radiative and nonradiative decay rate constants of the cluster in water, dioxane, and ethylene glycol (compared along with the data of phase-transferred clusters). Data for dioxane and ethylene glycol correspond to their solvent-rich aqueous solutions as in Figure 9. Both the radiative and nonradiative decay constants were significantly altered when the solvent was changed. The study was extended to other solvents and the maximum quantum yield obtained was 7% in DMSO with a 25 nm blueshift (see Figure S7 in Supporting Information 7). Solvent-dependent emission of Au₂₃ after phase transfer was also studied in alcohols. For this, 0.5 mL of the solution of the cluster in toluene was mixed with methanol, ethanol, propanol, butanol, and pentanol. The emission of the cluster increased with an increase in the chain length of the alcohol, reaching a maximum in butanol and a decreasing afterwards (Figure 9B). The quantum yield of the cluster in butanol was 13%. Thus the quantum yield of an Au₂₃ cluster can be increased significantly by selecting the proper solvents.

Since Au₂₂ and Au₂₃ clusters are highly fluorescent and water soluble, they can be used in biology-related experiments such as detection and imaging. These clusters may possess additional benefits over organic fluorophores and fluorescent semiconductor quantum dots. Whereas organic

fluorophores are prone to photobleaching, subnano clusters are photostable.^[17] Fluorescent semiconductor quantum dots are generally made of toxic elements like Cd and Pb, and they have to be covered with other inorganic or biological molecules to reduce the toxicity. Subnanoclusters composed of gold atoms, on the other hand, are likely to be biocompatible. Moreover, the cytotoxicity of the clusters is very low due to the low metallic content. Considering the above facts, an Au₂₃ cluster was used for imaging human hepatoma cells (HepG2). These are cancerous cells containing a large amount of biotin. Biotin is a cofactor in the metabolism of fatty acids. For the specific labeling of the cells, Au₂₃ clusters were functionalized with streptavidin following a 1-ethyl-3-(3-dimethylaminopropyl)carbodiimide (EDC) coupling reaction (shown in Scheme 2 and described in more detail in the Experimen-



Scheme 2. Schematic representation of the conjugation of streptavidin on Au₂₃SG₁₈ by EDC coupling.

tal Section). Since biotin strongly binds with streptavidin, the cells can be imaged using the fluorescence of the clusters. For this, HepG2 cells were allowed to grow to 80% confluency starting with 2×10^4 cells per well in 24-well tissue culture plates (in Dulbecco's Modified Eagle Medium (DMEM) supplemented with 10% fetal bovine serum (FBS) and incubated at 37°C in humidified atmosphere containing 5% CO₂). For the imaging experiment, the growth medium was removed and the cells were washed twice with phosphate buffered saline (PBS) to remove the dye phenol red and various chemical reagents such as salts and glucose present in the growth medium. After this, the cells were fixed with 3% paraformaldehyde. Two-hundred microliters of a concentrated aqueous solution of streptavidin-conjugated Au₂₃ was added and incubated for 2 h at room temperature. After incubation the cells were washed several times with PBS to remove the unbound clusters and were imaged by confocal fluorescence microscopy. A very intense red fluorescence was observed from the cells (see Figure 10). A control experiment was carried out to confirm the specificity of the streptavidin–biotin interaction. For this the fixed HepG2 cells were incubated with Au₂₃ clusters without any streptavidin conjugation for the same

period. No fluorescence was observed from the cells after washing (see Figure S8 in Supporting Information 8). This experiment confirms that the specific interaction of streptavidin and biotin allows the cluster to stain the cells. A detailed study of receptor-mediated uptake of these clusters functionalized with several biomolecules is underway and will be published elsewhere.

Conclusion

Three distinct near infrared (NIR)-emitting subnanoclusters of gold were synthesized from the widely explored subnanocluster Au₂₅SG₁₈. We have followed an elegant core-etching mechanism to synthesize these clusters. The clusters possess Au₂₂, Au₂₃, and Au₃₃ cores. This is the first report of the synthesis of Au₂₃ clusters. Whereas Au₂₂ and Au₂₃ are highly water soluble and brightly fluorescent with quantum yields of 2.5 and 1.3%, respectively, Au₃₃ is organic soluble and less fluorescent, with a quantum yield of 0.1%. Au₂₃ clusters exhibited quenching of fluorescence in the presence of Cu²⁺ ions and thus can be used as a Cu²⁺-detection tool. An aqueous- to organic-phase transfer of Au₂₃ was carried out by the phase-transfer reagent tetraoctylammonium bromide, and the cluster showed fluorescence enhancement in the organic medium. Fluorescence of the cluster shows environmental dependency with solvents and that emission-intensity increases with the hydrogen-bonding capacity of the solvent. The temperature response of the cluster has also been demonstrated. Au₂₃ clusters can be imaged using their fluorescence and are hopeful candidates for biologically motivated experiments such as detection and imaging because of their high quantum yield, photostability, and low cytotoxicity. Au₂₃ clusters have also been used to image human hepatoma (HepG2) cell lines.

Experimental Section

Materials: Tetrachloroauric acid trihydrate (HAuCl₄·3H₂O) was purchased from CDH, India. Glutathione (GSH), octanethiol (OT), 3-mercaptopropyl trimethoxysilane (MPTS), tetraoctyl ammonium bromide (TOABr), and sodium borohydride (NaBH₄) were purchased from Sigma–Aldrich. Streptavidin was purchased from Hi-Media Chemicals,

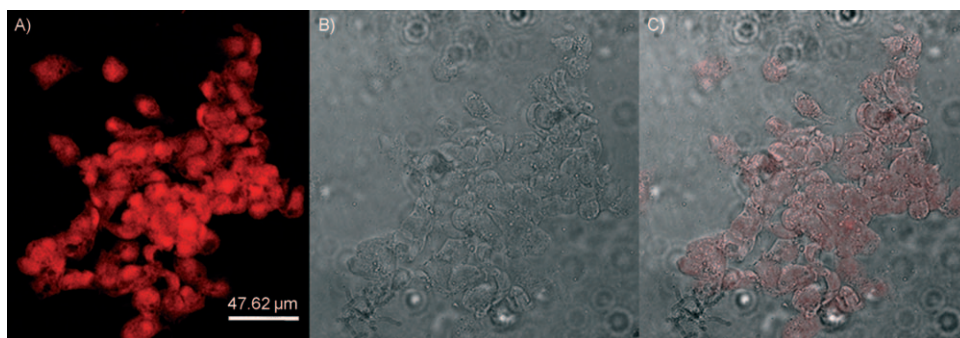


Figure 10. A) Fluorescence, B) bright field, and C) overlay of fluorescent and bright field images of human hepatoma (HepG2) cells stained with streptavidin-conjugated Au₂₃.

India. All chemicals were used as such without further purification. Triply distilled water was used throughout the experiments. Solvents used were of analytical grade.

Synthesis of glutathione-capped gold (Au@SG) clusters: Glutathione-capped gold clusters were synthesized according to a reported method.^[10] Reduced glutathione (GSH; 20 mM) was added to a solution of HAuCl₄·3H₂O (100 mL, 5 mM) in methanol. The mixture was then cooled to 0 °C in an ice bath for 30 min. An aqueous solution of NaBH₄ (25 mL, 0.2 M), cooled at 0 °C, was injected rapidly into this mixture under vigorous stirring. The mixture was allowed to react for another hour. The resulting precipitate was collected and washed repeatedly with methanol/water (3:1) through centrifugal precipitation and dried to obtain the Au@SG clusters as a dark brown powder. This product is a mixture of small nanoparticles and different clusters.

Synthesis of Au₂₅SG₁₈: Au₂₅SG₁₈ was synthesized from the as-prepared Au@SG clusters by ligand etching.^[12–15] The as-prepared Au@SG cluster was dissolved in water (25 mL). GSH was added (614 mg) and stirred at 55 °C. The reaction was monitored by optical absorption spectroscopy. Heating was discontinued when the absorption features of Au₂₅SG₁₈ appeared in the UV/Vis spectrum. This typically took 12 h of heating. The solution was centrifuged and methanol was added to the supernatant to precipitate the cluster. The precipitate was dried to obtain Au₂₅SG₁₈ clusters in the powder form. The prepared Au₂₅SG₁₈ shows characteristic UV/Vis, FTIR, TEM, and NMR spectroscopic features.

Synthesis of Au₂₃ clusters: The cluster was synthesized by interfacial etching. Au₂₅SG₁₈ clusters (10 mg) were dissolved in distilled water (10 mL). Octanethiol was taken in 1:8 ratio in toluene (5 mL). The mixture was stirred for 5 h at 25 °C. The aqueous and organic phases were separated and centrifuged. The organic layer was almost colorless.

Synthesis of Au₃₃ clusters: The cluster was also synthesized by interfacial etching. Au₂₅SG₁₈ clusters (10 mg) were dissolved in distilled water (10 mL). Octanethiol was taken in 1:8 ratios in toluene (5 mL). The mixture was stirred for 1 h at 55 °C. The organic layer, which was initially colorless, turned dark brown. The aqueous and organic phases were separated and centrifuged.

Synthesis of Au₂₂ clusters: The synthesis was carried out by single-phase etching: Au₂₅SG₁₈ clusters (10 mg) were dissolved in distilled water (10 mL). 3-Mercaptopropyl trimethoxysilane was added into the cluster solution at 1:2 ratio (cluster/thiol). The mixture was stirred for 7 h. The solution was centrifuged and the supernatant was separated.

Conjugation of streptavidin with Au₂₃: Conjugation of streptavidin with glutathione-protected Au₂₃ was carried out by EDC coupling. EDC (25 μL of 10 mM) prepared in triply distilled water was added to a mixture of Au₂₃ (2 mg) and streptavidin (1 mg) in triply distilled water (1 mL). The mixture was stirred for 3 h. The streptavidin-coated Au₂₃ was subjected to dialysis for 2 d with a water change after every 6 h.

Instrumentation: UV/Vis spectra were measured using a Perkin–Elmer Lambda 25 instrument in the range of 200–1100 nm. The Fourier transform infrared (FTIR) spectra were measured using a Perkin–Elmer Spectrum One instrument. KBr crystals were used as the matrix for preparing samples. Fluorescent measurements were carried out on Jobin Vyon NanoLog instrument. The band pass for excitation and emission was set as 5 nm. A WiTec GmbH Confocal Raman spectrometer, equipped with an argon-ion laser (532 nm) was used as the excitation source to collect the fluorescence images of the solid films. The laser was focused onto the sample using a 100× objective, with the signal collected in a back-scattering geometry. The signal, after passing through a super-notch filter, was dispersed using 150 grooves mm⁻¹ grating onto a Peltier cooled charge-coupled device (CCD), which served as the detector. The sample mounted on a piezo stage was scanned with the signal collected at every pixel. For the images displayed, the scan area was divided into 100×100 pixels for spectral image acquisition. X-ray photoelectron spectroscopy (XPS) measurements were conducted using an Omicron ESCA Probe spectrometer with polychromatic MgKα X-rays (*hν* = 1253.6 eV). The samples were spotted as drop-cast films on a sample stub. Constant analyzer energy of 20 eV was used for the measurements. Matrix-assisted laser-desorption/ionization (MALDI) mass spectrometric studies were conducted using a Voyager-DE PRO Biospectrometry Workstation from Applied Biosys-

tems. For MALDI-TOF MS, a pulsed nitrogen laser of 337 nm was used for the studies. Mass spectra were collected in positive-ion mode and were averaged for 50 shots. Fluorescence transients were measured and fitted by using a commercially available spectrophotometer (LifeSpec-ps) from Edinburgh Instruments, U.K. (80 ps instrument response function (IRF)). The clusters were excited at 409 nm and the emission decays were collected at 630 nm. Energy-dispersive analysis of X-rays (EDAX) was carried out using a FEI QUANTA-200 SEM instrument, and the samples were prepared on conducting ITO glass plates. A Leica TCS SP2-AOBS confocal microscope was used for imaging the cells by excitation using the 514 nm laser. Emission between 600 and 800 nm was collected.

Acknowledgements

We thank the Department of Science and Technology, Government of India for constantly supporting our research program on nanomaterials.

- [1] J. Zheng, R. M. Dickson, *J. Am. Chem. Soc.* **2002**, *124*, 13982.
- [2] C. M. Ritchie, K. R. Johnsen, J. R. Kiser, Y. Antoku, R. M. Dickson, J. T. Petty, *J. Phys. Chem. C* **2007**, *111*, 175.
- [3] A. S. Patel, C. I. Richards, J.-C. Hsiang, R. M. Dickson, *J. Am. Chem. Soc.* **2008**, *130*, 11602.
- [4] J. Yu, S. A. Patel, R. M. Dickson, *Angew. Chem.* **2007**, *119*, 2074; *Angew. Chem. Int. Ed.* **2007**, *46*, 2028.
- [5] J. Zheng, P. R. Nicovich, R. M. Dickson, *Annu. Rev. Phys. Chem.* **2007**, *58*, 409.
- [6] J. Zheng, J. T. Petty, R. M. Dickson, *J. Am. Chem. Soc.* **2003**, *125*, 7780.
- [7] J. Zheng, C. W. Zhang, R. M. Dickson, *Phys. Rev. Lett.* **2004**, *93*, 077402.
- [8] H. Duan, S. Nie, *J. Am. Chem. Soc.* **2007**, *129*, 2412.
- [9] T. G. Schaaff, G. Knight, M. N. Shafiqullin, R. F. Borkman, R. L. Whetten, *J. Phys. Chem. B* **1998**, *102*, 10643.
- [10] Y. Negishi, K. Nobusada, T. Tsukuda, *J. Am. Chem. Soc.* **2005**, *127*, 5261.
- [11] Y. Shichibu, Y. Negishi, T. Tsukuda, T. Teranishi, *J. Am. Chem. Soc.* **2005**, *127*, 13464.
- [12] Y. Shichibu, Y. Negishi, H. Tsunoyama, M. Kanehara, T. Teranishi, T. Tsukuda, *Small* **2007**, *3*, 835.
- [13] M. A. Habeeb Muhammed, T. Pradeep, *Chem. Phys. Lett.* **2007**, *449*, 186.
- [14] E. S. Shibu, M. A. Habeeb Muhammed, T. Tsukuda, T. Pradeep, *J. Phys. Chem. C* **2008**, *112*, 12168.
- [15] M. A. Habeeb Muhammed, A. K. Shaw, S. K. Pal, T. Pradeep, *J. Phys. Chem. C* **2008**, *112*, 14324.
- [16] M. Zhu, E. Lanni, N. Garg, M. E. Bier, R. Jin, *J. Am. Chem. Soc.* **2008**, *130*, 1138.
- [17] C.-A. J. Lin, T.-Y. Yang, C.-H. Lee, S. H. Huang, R. A. Sperling, M. Zanella, J. K. Li, J.-L. Shen, H.-H. Wang, H.-I. Yeh, W. J. Parak, W. H. Chang, *ACS Nano* **2009**, *3*, 395.
- [18] J. I. Gonzalez, T.-H. Lee, M. D. Barnes, Y. Antoku, R. M. Dickson, *Phys. Rev. Lett.* **2004**, *93*, 147402.
- [19] T.-H. Lee, J. I. Gonzalez, J. Zheng, R. M. Dickson, *Acc. Chem. Res.* **2005**, *38*, 534.
- [20] M. A. Habeeb Muhammed, S. Ramesh, S. S. Sinha, S. K. Pal, T. Pradeep, *Nano Res.* **2008**, *1*, 333.
- [21] X. Liu, C. Li, J. Xu, J. Lv, M. Zhu, Y. Guo, S. Cui, H. Liu, S. Wang, Y. Li, *J. Phys. Chem. C* **2008**, *112*, 10778.
- [22] J. Xie, Y. Zheng, J. Y. Ying, *J. Am. Chem. Soc.* **2009**, *131*, 888.
- [23] Y. Shichibu, Y. Negishi, T. Tsukuda, T. Teranishi, *J. Am. Chem. Soc.* **2005**, *127*, 13464.
- [24] C. N. R. Rao, K. P. Kalyanikutty, *Acc. Chem. Res.* **2008**, *41*, 489.
- [25] C. N. R. Rao, G. U. Kulkarni, P. J. Thomas, V. V. Agarwal, P. Saravanan, *J. Phys. Chem. B* **2003**, *107*, 7391.

- [26] K. P. Kalyanikutty, U. K. Gautam, C. N. R. Rao, *Solid State Sci.* **2006**, *8*, 296.
- [27] K. V. Mrudula, T. Udaya Bhaskara Rao, T. Pradeep, *J. Mater. Chem.* **2009**, *19*, 4343.
- [28] M. Zhu, C. M. Aikens, F. J. Hollander, G. C. Schatz, R. Jin, *J. Am. Chem. Soc.* **2008**, *130*, 5883.
- [29] N. Sandhyarani, M. P. Antony, G. Panneer Selvam, T. Pradeep, *J. Chem. Phys.* **2000**, *113*, 9794.
- [30] P. Pyykkö, N. Runeberg, *Angew. Chem.* **2002**, *114*, 2278; *Angew. Chem. Int. Ed.* **2002**, *41*, 2174.
- [31] P. Pyykkö, *Angew. Chem.* **2004**, *116*, 4512; *Angew. Chem. Int. Ed.* **2004**, *43*, 4412.
- [32] X. Lua, H-Y. Tuanb, B. A. Korgelc, Y. Xia, *Chemistry* **2008**, *14*, 1584.
- [33] J. Cyriac, V. R. Rajeevkumar, T. Pradeep, *Chem. Phys. Lett.* **2004**, *390*, 181.
- [34] T. G. Schaaff, *Anal. Chem.* **2004**, *76*, 6187.
- [35] B-K. Pong, B. L. Trout, J-Y. Lee, *Langmuir* **2008**, *24*, 5270.
- [36] S. Jeong, M. Achermann, J. Nanda, S. Ivanov, V. I. Klimov, J. A. Hollingsworth, *J. Am. Chem. Soc.* **2005**, *127*, 10126.
- [37] R. C. Dougherty, *J. Chem. Phys.* **1998**, *109*, 7372.

Received: May 27, 2009
Published online: August 26, 2009